Dense Plasma Focus: physics and applications (radiation material science, single-shot disclosure of hidden illegal objects, radiation biology and medicine, etc.)

2015 J. Phys.: Conf. Ser. 591 012020

(http://iopscience.iop.org/1742-6596/591/1/012020)

Journal of Physics: Conference Series **591** (2015) 012020 doi:10.1088/1742-6596/591/1/012020

Dense Plasma Focus: physics and applications (radiation material science, single-shot disclosure of hidden illegal objects, radiation biology and medicine, etc.)

V.A. Gribkov[1,2,3,4], R. Miklaszewski[1], M. Paduch[1], E. Zielinska[1], M. Chernyshova[1], T. Pisarczyk[1], V.N. Pimenov[2], E.V. Demina[2], J. Niemela[3], M.-L. Crespo[3], A. Cicuttin[3], K. Tomaszewski[5], M.J. Sadowski[1,6], E. Skladnik-Sadowska[6], K. Pytel[6], A. Zawadka[6], G. Giannini[7], F. Longo[7], A. Talab[8], S.E. Ul'yanenko[9]

[1]Institute of Plasma Physics and Laser Microfusion, Warsaw, Poland,
[2]A.A. Baikov Institute of Metallurgy and Material Sciences, Russ. Ac. Sci., Moscow, R.F.
[3]The Abdus Salam International Centre for Theoretical Physics, Trieste, Italy
[4]A.I. Alikhanov Institute of Theoretical and Experimental Physics, Moscow, R.F.
[5]ACS Ltd., Warsaw, Poland
[6]National Centre for Nuclear Research, 05-400 Otwock, Poland
[7]Department of Physics, University of Trieste, Trieste, Italy
[8]Atomic Energy Authority, NRC, Plasma Physics and Nuclear Fusion Department, Egypt
[9] Medical Radiological Research Center, Russ. Ac. Med. Sci., Obninsk, Kaluga region, R.F.

E-mail: gribkovv@rambler.ru

Abstract. The paper presents some outcomes obtained during the year of 2013 of the activity in the frame of the International Atomic Energy Agency Co-ordinated research project *"Investigations of Materials under High Repetition and Intense Fusion-Relevant Pulses"*. The main results are related to the effects created at the interaction of powerful pulses of different types of radiation (soft and hard X-rays, hot plasma and fast ion streams, neutrons, etc. generated in Dense Plasma Focus (DPF) facilities) with various materials including those that are counted as perspective ones for their use in future thermonuclear reactors. Besides we discuss phenomena observed at the irradiation of biological test objects. We examine possible applications of nanosecond powerful pulses of neutrons to the aims of nuclear medicine and for disclosure of hidden illegal objects. Special attention is devoted to discussions of a possibility to create extremely large and enormously diminutive DPF devices and probabilities of their use in energetics, medicine and modern electronics.

1. Introduction

The most important effect ruled the physical processes in a DPF device [1] is the "current abruption" (CA) phenomenon [2, 3]. During this transient event (occurring in the ps time scale) a plasma diode is

produced, which switches stored energy over to the beams of fast particles – electrons and ions. These fast particles produce extremely bright flashes of X-rays and neutrons. It gives us an opportunity to make *heavy* science by means of *light* technology.

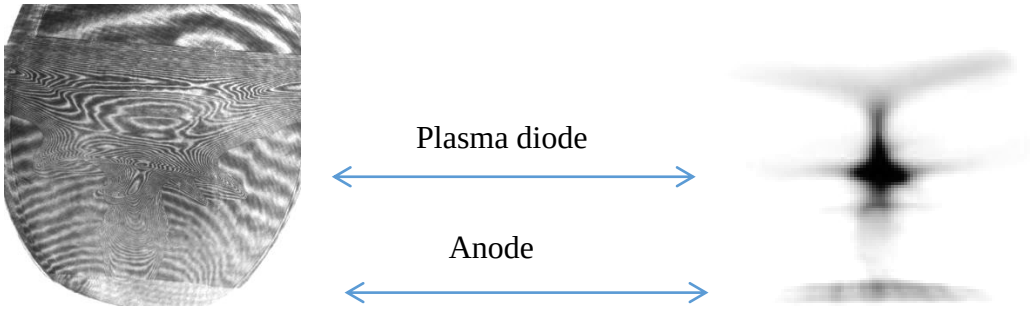

Figure 1. 1-ns laser interferometric (a) and self-luminescence (b) pictures of the pinch during the plasma-diode formation on the plasma column.

Value of current of fast electrons I_{fe} can be sharply inferred from X-ray dosimetry, i.e. by measuring an X-ray dose ($D = F \times \tau_x$) where F is energy flux with its spectral distribution (depends on U_{eff}), anode material (Z) and pulse duration (τ_x):

$$F \sim k_x Z U_{eff}^{\,2} I_{fe} \text{ where } k_x = 10^{-9} \text{ [W/(V}^2\text{A)]}$$

Current of fast ions I_{fi} can be estimated by measuring neutron yield taking into consideration size (V_{pinch}) and density (n_{pl}) of the pinch plasma, time duration of the fast ions pulse (τ_{fi}) with the corresponding cross-section (σv) and magnetization degree of the ions k_m (5…10 [2, 3]):

$$Y_n \sim n_{pl} N_{fi} (\sigma v) V_{pinch} \tau_{fi} = n_{pl} (I_{fi} / e v_{fi} S_{fi}) (\sigma v) V_{pinch} \tau_{fi}$$

According to these measurements and formulae both types of currents (of fast electrons and high-energy ions) *sequentially in time* substitute almost the overall discharge current in DPF during the course of the CA phenomenon.

In particular one may see that the total number of fast deuterons generated in the PF-1000 facility [2, 3] is about 10^{18}. It means that a DPF is a good accelerator (efficiency of the bank energy conversion to the overall energy of the fast ion beam is $\eta \sim 10\%$) but a bad target (the product of density and dimensions is $n_{pl} \times l_{pinch} << 1/\sigma_{fusion}$, and the Lawson criterion is about $n_{pl}\tau \sim 10^{11}$ [cm^{-3}s]).

2. Medium-sized DPF and their applications

At present time the following two types of energy transfer from the primary source to the load are mainly used: capacitive storage with the circuit closer and inductive storage with the circuit interrupter:

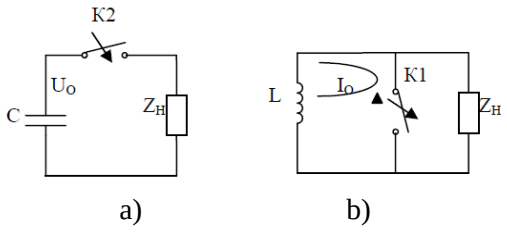

Figure 2. Capacitive and inductive storage systems with current closer and current interrupter correspondingly.

In the second case where L = const and when the load $Z_H \approx L_H$ in the most favorite case (when $L \approx L_H$) according to the Ampere's law the two portions by ~ ¼ part of the overall energy accumulated first in the magnetic storage system L will correspondingly be preserved in this primary storage L and another ¼ will be transferred to the load $Z_H \approx L_H$, whereas ½ part of it will be lost inside the breaker K_1.

In the medium-sizes DPF devices (with energies in the capacitor banks from 1 kJ till 100 kJ) one can reach the optimal (variable!) ratio of external (L_{ext}) and internal (L_{int}) inductances. Namely in the beginning of the discharge (at the breakdown phase) $L_{ext} >> L_{int}$, but during the pinching stage the ratio becomes just opposite $L_{ext} << L_{int}$ due to a variation of the dynamical internal inductance.

Moreover, during the maximal compression, when our pinch represents by itself a plasma inductive storage, the current breaker is situated *inside* the pinch (formation of a plasma diode). Energy that is usually lost in the external current interrupter in the classical scheme (*K1* in Fig. 2) is converted within the DPF pinch into beams of fast electrons and ions.

Because of the above two unique features (the dynamical change of the ratio L_{ext} / L_{int} and the active role of the current interrupter) it is possible to transfer from "plasma inductive storage" to the "load" (in the ideal theoretical approximation) up to 100% of the energy of azimuth magnetic field of the pinch, which is of the order of primary energy stored in the capacitor bank.

It is interesting to compare parameters of the discharge of the PF-6 device (IPPLM, Warsaw, Poland; C_{bank} = 32 μF, $E_{bank} \approx$ 6.4 kJ, $I_{max} \approx$ 760 kA, $\omega_{disch} \approx 10^6$ c^{-1}, $L_{pinch} \approx$ 30 nH): $\rho = \sqrt{L_{pinch}/C_{bank}} \approx Z_{pinch} = \omega L \approx R_{EMH} = 30uc \approx$ 30 mΩ (where u – current drift velocity, c – speed of light), i.e. the wave impedance ρ, the impedance of the pinch ($Z_{pinch} = \omega L$) and the electron magneto-hydrodynamic resistance ($R_{EMH} = 30uc$) [4] of the plasma diode are equal. Thus matching of all important circuit characteristics is excellent.

Such an apt combination of electrical parameters of the circuit facilitates a broad range of applications of these devices in various fields of science and technology with a very high efficiency of use of ionizing radiations generated by them.

Among these areas we shall present recent results obtained in radiation material science (testing of materials perspective for use in nuclear fusion devices), in unveiling of hidden fissile illegal items in a luggage, in dynamic quality control of machines and mechanisms in a course of their operation, in radiation biology (radio-enzymology), and in nuclear medicine (pulsed neutron treatment of cancer). The most important advantages in the applications of a DPF are demonstrated in those cases where nanosecond radiation pulses are used in pulsed radiation physics/chemistry/biology in their "perfect sense" [5], i.e. when micro-volumes of activity of secondary particles are overlapped during a time interval, which is short compared with the reciprocal physical/chemical/biological process. This time we used for irradiation 4 devices: PF-6 and PF-1000 (both IPPLM, Poland), the "Bora" facility (ICTP, Italy) and PF-5M (IMET, R.F.).

2.1. *Radiation material science*

In the past year we have irradiated targets made of different materials counted as the perspective ones for implementation of them in nuclear fusion reactors (Ti-based alloys, Mo, carbon-based composites CFC and SiC, low-activated stainless steels – all prepared in IMET, R.F., and in particular the tungsten-based material, identical samples of which were supplied to the participants of the IAEA CRP by the team of the FZJ, Juelich, Germany). Our main aim in these experiments was to test the above samples by fusion relevant pulses of hot plasma and fast ion streams generated in DPF. Results of their analytical examination after irradiation are presented in Fig. 3.

Fig. 3*a* shows a W-sample's photo after irradiation. One may clearly see a region (in the low-right corner) of the action of strong beam of fast deuterons (average energy is E_d ~ 100 keV). The rest part of the sample was irradiated mainly by a hot plasma stream (T_e ~ 300 eV, $v_{pl} \sim 2\times10^7$ cm/s). In the border between these zones an optical microscopy (*b*) has shown pores and ridges in the plasma-action area (power flux density here is estimated as ~10^9 W/cm^2, penetration depth of plasma ions is about 1 nm). Remelted surface in the fast ion beam action part of the sample with cracks (fracturing pattern) on

it is seen better in the SEM picture (*c*). Roughness of the surface was measured by atomic-force microscopy (Fig. 3*d*). In Fig. 3*e* we have presented a result obtained by an X-ray micro-tomographic computer technique using 150 kV HAMAMTSU micro-focus X-ray source L8121-03 and COBRA micro CT software. The picture is a cross-section of a Ti foil taken in a certain part of the sample after its irradiation. In the slice one may see some imperfections that are probably a result of a damage produced by a shock wave generated and penetrated through the foil after the action of the beam of fast deuterons.

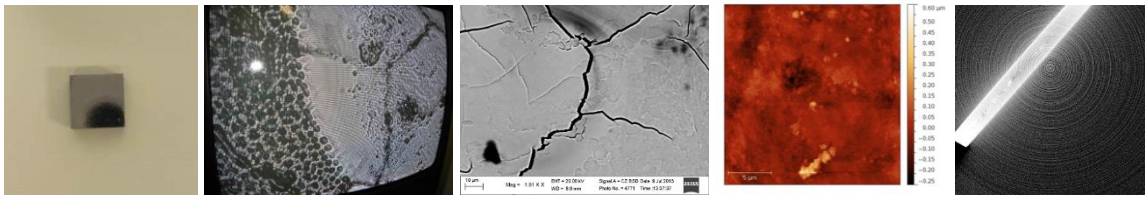

a) b) c) d) e)

Figure 3. Macroscopic image *(a)* of the tungsten specimen No. 40 after its irradiation in DPF, an optical microscopic picture of it *(b)* at the border between zones of irradiation by hot plasma and fast ion beam, a scanning electron microscopic view *(c)* of the part of the same sample with the strongest action of the ion beam, an atomic force microscopy *(d)* of the sample with its roughness, as well as one cross-section of the Ti foil made by the X-ray micro-tomography *(e)*.

It is important to note that we can investigate the samples not only *after* their irradiation by various analytical methods. In fact we are able *to monitor the irradiation process itself* with high temporal, spatial and spectral resolution by laser interferometry (Fig. 4 and 5) or by registering self-luminescence of plasma (Fig. 1*b* and Fig. 6).

Processing of an interferometric picture taken at the beginning of the formation of secondary plasmas produced on the anode by the self-focused beam of fast electrons (on the left side) and by the divergent stream of fast ions on the stainless steel plate of 2-mm thickness (on the right side) is shown in Fig. 5.

From processing of the interferometric pictures one may see that in secondary plasma produced by the electron beam near the anode surface the upper measured limit of density is higher than in secondary plasma produced by the ion beam. It results from the fact that the lateral dimension of the first type of plasma is small compared with the second one. In its turn it is a consequence of self-focusing of the electron beam in opposite to the divergent ions beam. Thus the upper limit is determined by crowding of interferometric fringes.

From Fig. 6 one may see that in the first period of time after the CB phenomenon our spectrometer registers mainly deuterium plasma lines (D_α, D_β…). This is our "primary" plasma generated in the pinch and colliding with the target. Then at the moments near the second microsecond after CA secondary plasma is generated near the target (in this case a sample of SiC).

One may see here mainly lines of the target's material (C and Si). The degree of ionization (e.g. an observation of C IV lines) confirms the high value of secondary plasma temperature that was deduced earlier from the velocity of its expansion. In the late stages the spectrometer registers a mixture of both substances.

In the very late stage (10μs after CA phenomenon) at using for an irradiation in the PF-1000 facility a thin (2 mm) sheet of stainless steel we were able to register a shock wave generated inside the target by the ion beam and escaping subsequently from the rear side of the blade (see Fig. 7).

What is of a particular interest in the picture – it is a "post pinch" that continues to exist during a very long period of time (much more than 10 microsecond after CA phenomenon).

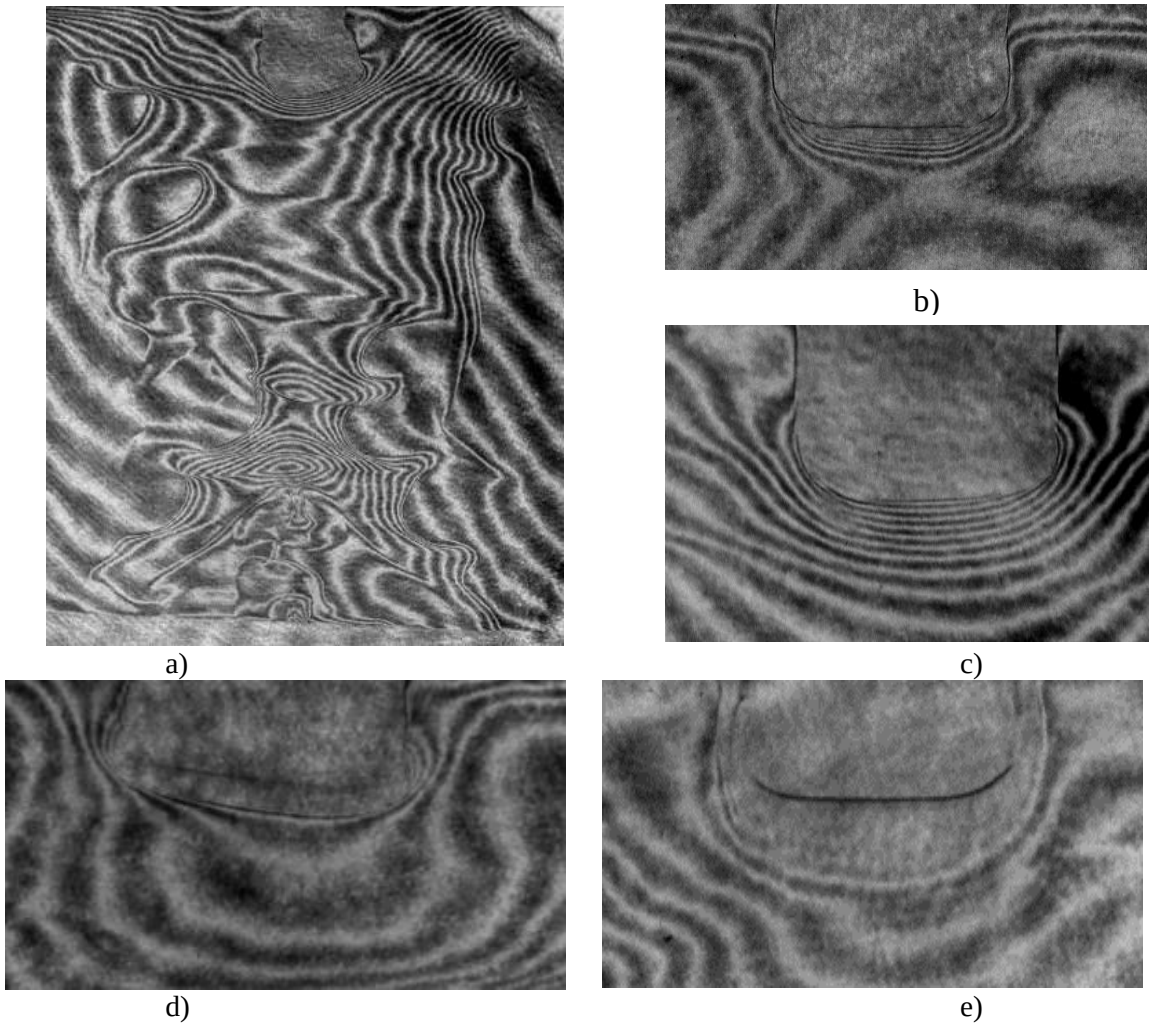

Figure 4. Laser interferometric images of target's plasma (specimen's material – SiC) taken at 4 consecutive time moments (temporal resolution – 1 ns): beginning of the secondary plasma formation (*a* and *b*), well-developed secondary plasma cloud (*c*), beginning of the formation of the unloading wave (*d*) and well-developed unloading wave (*e*).

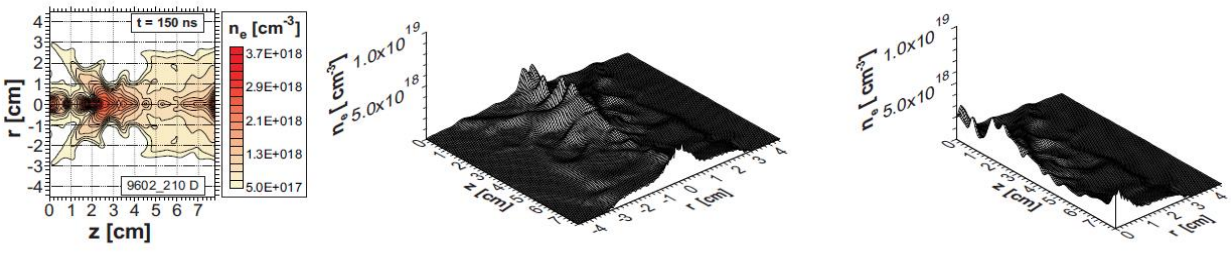

Figure 5. Electron density distribution (*a*) according to the processing of the interferometric image (Fig. 4 *a*) of the interaction of the powerful electron (left-hand side) and ion (right-hand side) streams with targets: *b*) – two-dimensional map, *c*) – cross-section along the Z-axis.

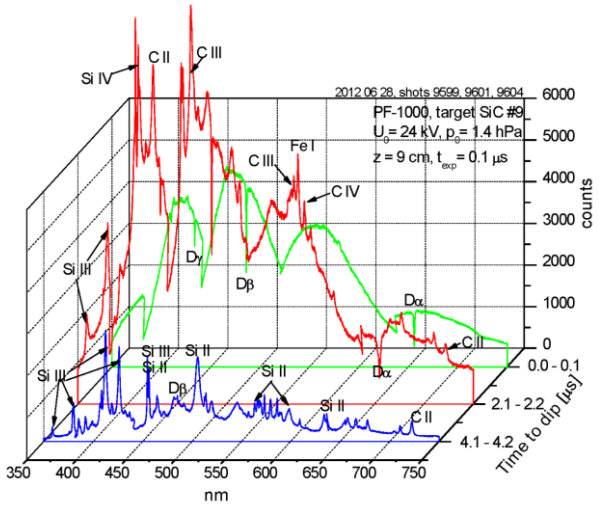

Figure 6. Time evolution of the secondary plasma spectrum taken in visual range with temporal resolution equal to 100 ns.

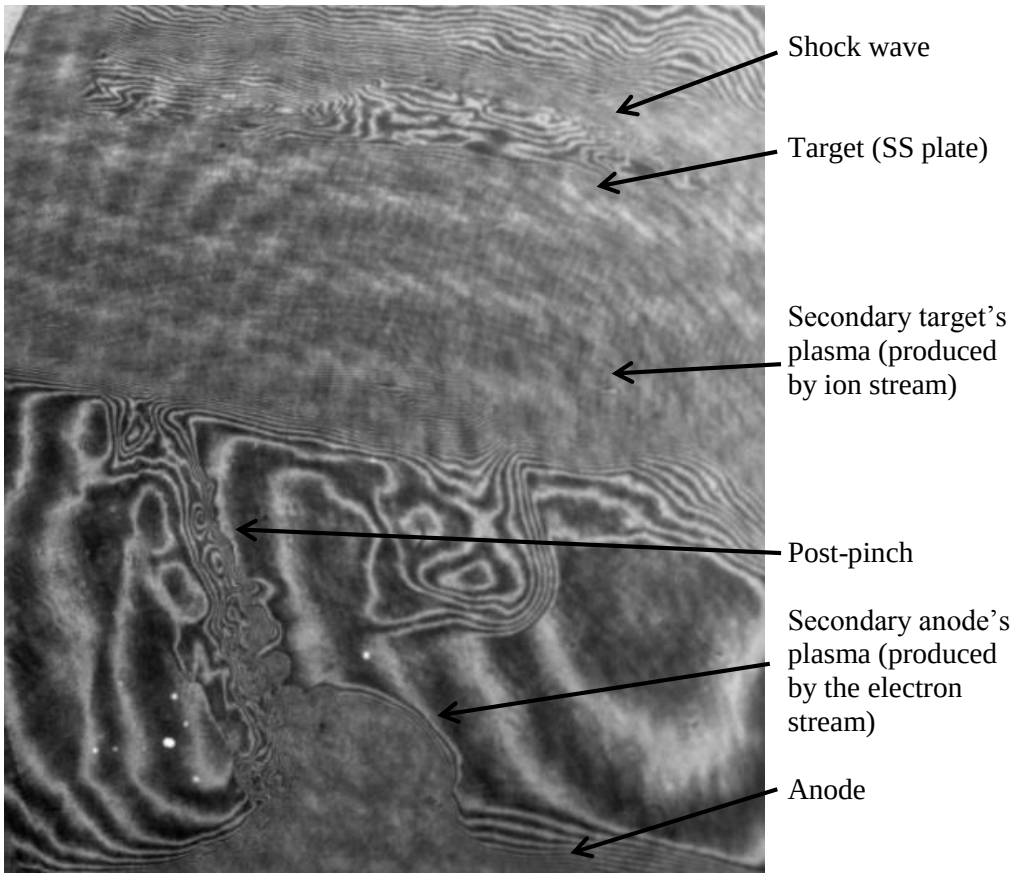

Figure 7. Late stage of the secondary plasmas/pinch development (10 µs after the current dip) taken at the irradiation of thin stainless plate with a post-pinch and a shock wave escaping from the rear side of the plate.

Together with the data of measurements provided in the collector part of the DPF chamber (in the PF-1000 facility) by a set of magnetic probes we have learned that at this configuration with the large-size metallic blade placed in a distance of ~ 10 cm from the anode the pinch is separated from the main electrical circuit and works as a torus-like self-organized magnetic storage dissipating its energy during period of time of the order: $\Delta t \sim L/R$ (~ 100 μs for the PF-1000), where L is the post-pinch inductance and R is its resistivity. This result is supported by the spectroscopic investigations (of the type of Fig. 6).

2.2. *Microlithography and micromachining*

DPF can be effectively used by means of irradiating of photoresists with soft X-rays for microlithography (with Ne-filled chamber) [6] and micromachining [7], i.e. in manufacturing of 3D structures (with Ar-filled chamber).

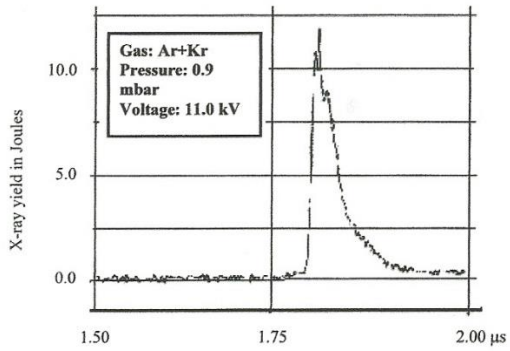

Figure 8. Soft X-ray pulse obtained at the DPF operation with Ar-Kr gas mixture.

In Fig. 8 one may see an X-ray pulse obtained in the second case whereas Fig. 9 is a picture of a structure obtained in such schemes at the National Institute of Education (Singapore) with a photoresist with chemical amplification.

As it will be seen from the subsequent part this micromachining technique can in principle be used for manufacturing of super-miniature DPF devices.

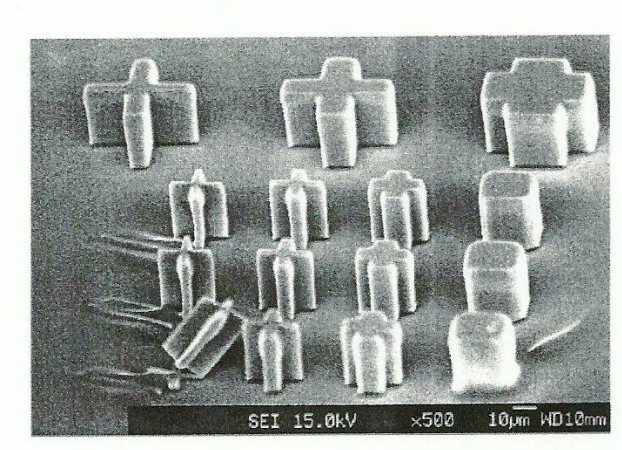

Figure 9. 3-dimentional structure obtained in the wave-length rang near 0.4 nm at the photoresist with chemical amplification.

2.3. *Dynamic quality control of machines and mechanisms in a course of their operation*

DPF as a source of very bright nanosecond pulses X-rays and neutrons can be implemented for the dynamic quality control of machines and mechanisms in a course of their operation. In principle these two types of radiation are additive and can provide information on dissimilar features of the object under irradiation (e.g. X-rays can give us information about high-Z materials whereas neutrons – about low-Z – light – parts of it). At this stage we used hard X-ray flash generated by "Bora" device.

Spatial resolution of an image of a mechanism's detail (turbine's blade, car tire, piston of a car engine, etc.) taken during its operation by a flash of the hard X-Ray radiation from DPF determined by a number of factors:

- Pulse duration of X-Rays (ns)
- Size of the source of X-Rays and its remoteness from an object (< 100 μm, usually from 10 cm to a few meters)
- Diffraction (wavelength, distance)
- Contrast degree of an object's detail to be visualized (spectrum of hard X-Rays)

Theoretically for DPF it could be ~ 1 μm in a 10-cm distance at the rotation speed of a machine's part ~ 10,000 rotations per minute.

We have made several experiments in this field including the last one with a plastic fan during its operation. In the below Fig. 10 one may see the overview of the experiment (*a* and *b*) and two pictures taken with soft X-rays irradiating by the "Bora" device (ICTP) – one in a static position of the fan (*c* - 7 shots of DPF) and the other one during the fan's rotation (*d* – one shot of the "Bora" device). It is possible to see that the dynamic picture does not differ from the static one.

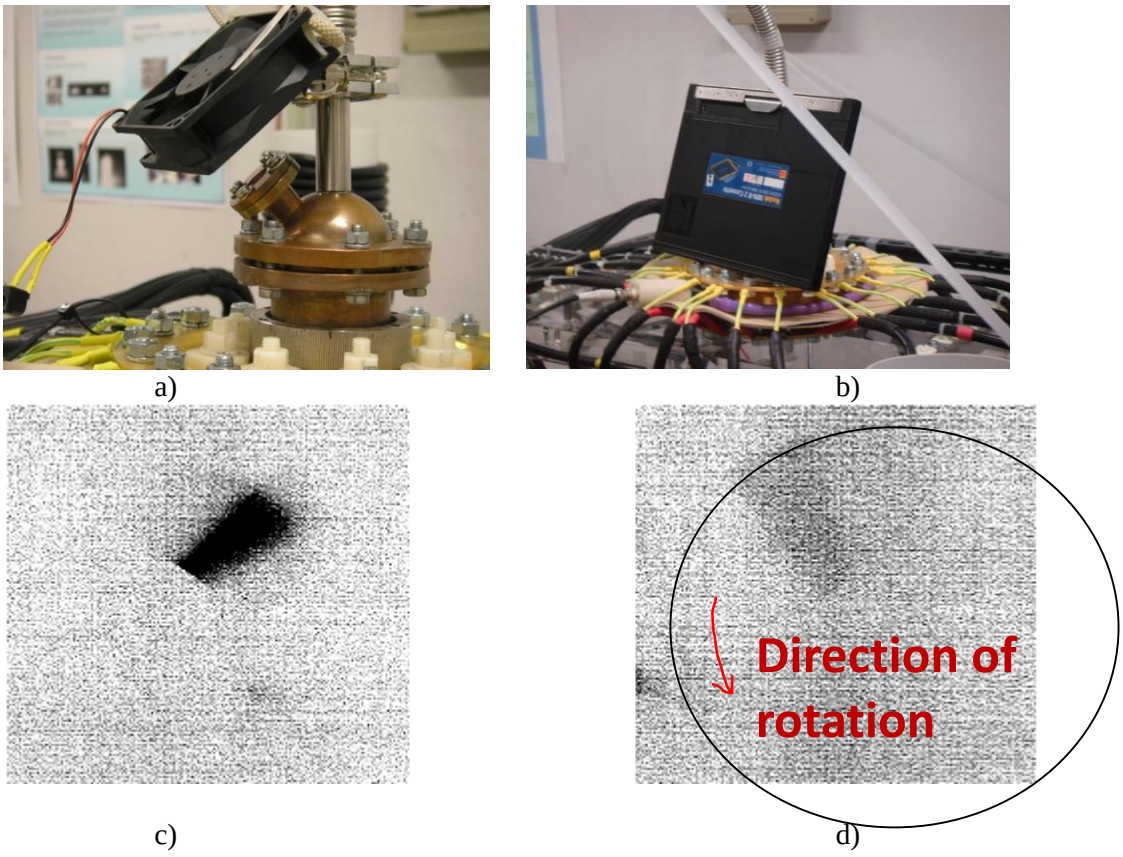

Figure 10. The arrangement of the experiment on the dynamic quality control (*a* and *b*) and two X-ray pictures of a fan in its static (*c*) and dynamic (*d*) states.

This technique opens opportunities in a dynamic quality control of machines during their operation. It can be important e.g. in mass production and defectoscopy of car tires moving in the conveyer, in a woodworking industry, in a quality control of turbine's blades when a "closed" defect might be visualized during the rotation because of a centrifugal force that may "open" this crack.

2.4. *Radiation chemistry/biology*

Formerly in these experiments enzymes were irradiated *in vitro* with various *doses, dose power and spectral range* by *X-Ray photons.*

We have found here a very large (4 orders (!) of magnitude) *difference in doses for the enzyme activation/inactivation* by their irradiation with X-Rays from DPF compared with the same procedure using an isotope source (Cs^{137}) [8].

However our attempts to find the same effect with *neutron irradiations* produced by DPF, neutron generators and pulsed fission reactor BARS were failed.

In these experiments the maximum of 14-MeV neutron tissue kerma obtained with DPF devices was 0.8 Gy, whereas for X-rays it was 0.5 Gy. ING-104 pulsed neutron generator is a Dense Plasma Focus (DPF) device, which serves as a source of nanosecond pulses of X-rays and neutron radiation. Pulses duration ranges from 20 to 30 ns. Below we present results of cytogenetic effects of mixed X-ray and 14-MeV neutron radiation of nanosecond pulses on human lymphocytes (Fig. 11 and 12).

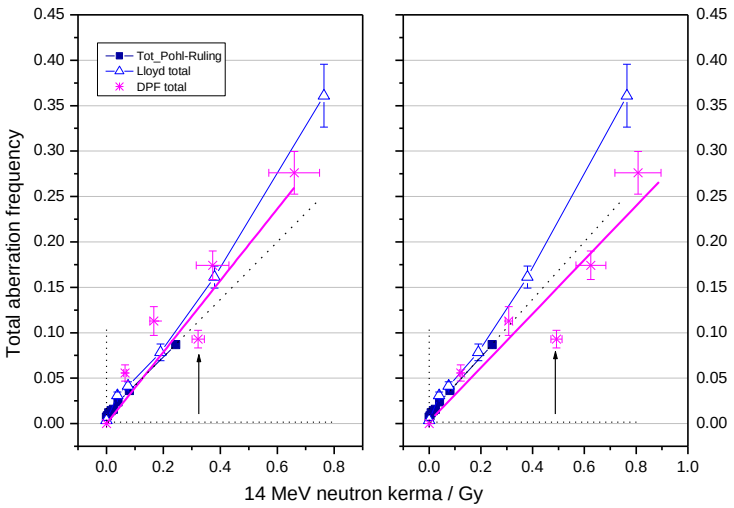

Figure 11. Dose curves of the total chromosomal aberration yield in human lymphocytes irradiated with 14 MeV neutrons. Left panel – neutron kerma was calculated using ^{237}Np fission detector; right panel – neutron kerma was calculated using SIVN 61 neutron yield monitor with activation silver detector. Linear regression equation are $Y_{tot} = (0.041 \pm 0.009) + (0.36 \pm 0.022)K$ and $Y_{tot} = (0.021 \pm 0.01) + (0.28 \pm 0.028)K$, respectively. DPF – Dense Plasma Focus.

5 plastic tubes with blood samples were placed in a cylinder plastic container using special holder. Diameter (inner) of the container was 55 mm, diameter of each tube was 10 mm, and wall thickness was 1 mm. Since DPF produced only 1 pulse every 10 minutes, to prevent damage reparation between pulses container was filled with melting ice and then it was mounted on the top of the plasma focus discharge chamber. Fission detectors with ^{237}Np were placed outside the container opposite to each tube with blood. Neutron kerma was calculated using two types of detectors – the above-mentioned ^{237}Np detector and the activation silver detector, which was the part of neutron yield monitor SIVN 61. In calculating kerma we supposed that neutron flux decreased according to $1/R^2$ law and the plasma focus neutron source was 25 mm below the top of the discharge chamber. To estimate the influence of scattered neutrons on detectors indications a Monte Carlo calculations were made with MCNP-4b code.

X-rays doses were measured with a 27012 clinical dosimeter (Dresden). The blood samples were received 16 pulses in total.

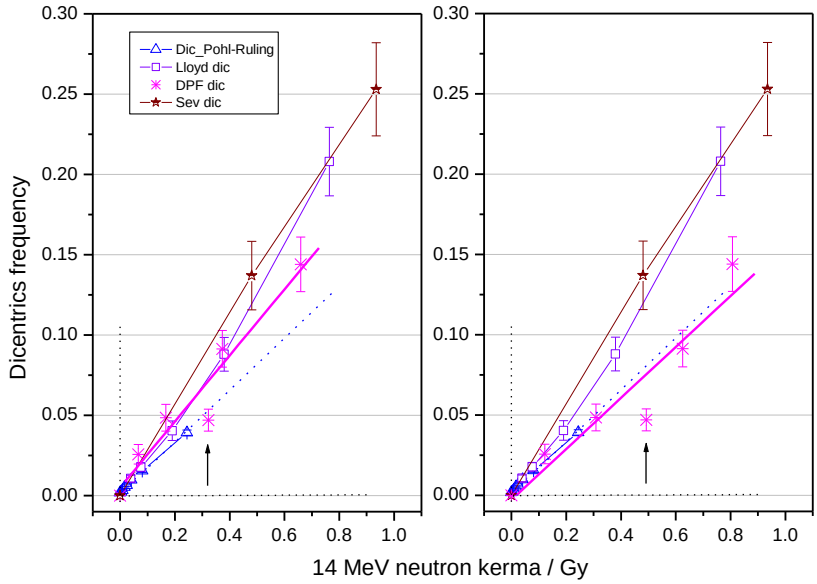

Figure 12. Dose curves of the dicentric chromosome yield in human lymphocytes irradiated with 14-MeV neutrons. Left panel – neutron kerma was calculated using ^{237}Np fission detector; right panel – neutron kerma was calculated using SIVN 61 neutron yield monitor with activation silver detector. Linear regression equation are $Y_{dic} = (0.012\pm0.006) + (0.21\pm0.026)K$ and $Y_{dic} = (0.005\pm0.01) + (0.15\pm0.026)K$, respectively.

At least three conclusions may be inferred from the above figures:

- First, the major contribution to the cytogenetic effect of the DPF neutron generator radiation is made by *neutrons.*

- Second, pulsed neutron radiation of *short, nanoseconds, duration is as effective as it is at continuous mode of neutron radiation, at least, within the mutual experimental uncertainties at its relatively high values (< 10^8 Gy/min)* for 14-MeV neutrons. It gives hope of applicability of DPF for the potential methods of neutron therapy *instead of cumbersome, expensive and dangerous nuclear reactors.*

- Third, our estimations made for boron-capture neutron therapy with Li ions and α-particles as products of nuclear reactions with their mean-free paths (6 and 9 μm respectively) have shown that for the above-mentioned overlapping of activity of the nuclear reaction products we need a flux of neutrons ~ 10^{12} n/cm^2.

2.5. *Nuclear medicine (pulsed neutron treatment of cancer)*

The main ideas to expect the same effects as with X-rays namely in malignant cells enriched with boron to higher degree compared with sound cells are as follows:

- Usage of *epithermal neutrons* (high cross-section, deep penetration)

- S*imultaneous destruction* of both spirals of DNA of malignant cells during the ns period of time by a high-density neutron flux (a “shock-like action” at a double-strand rupture)

- *Threshold-like behavior* of radiation damage of malignant cells due to the overlapping of micro-volumes of activity of free radicals and nuclear reaction products only in malignant cells.

All these opportunities might open ways for a *low-dose therapy* of cancer.

It is clear that to gain these opportunities we have to change spectrum of fast neutrons from DPF into spectrum with a large quantity of epithermal neutrons. However we must:

1) Not to lose too many neutrons

2) Not to increase neutron pulse duration too much (should be < 1 μs that is the time duration of biochemical reactions with free radicals).

In this work we focus on the development of a detailed simulation of interaction of short-pulse radiation generated by a DPF with tissue to estimate the absorbed dose by the cells for this dynamic case. The simulation was carried out by means of the Geant4 code [9], a toolkit to simulate the interaction of radiation with matter, originally developed for nuclear and particle physics. One of the results is presented in Fig. 13.

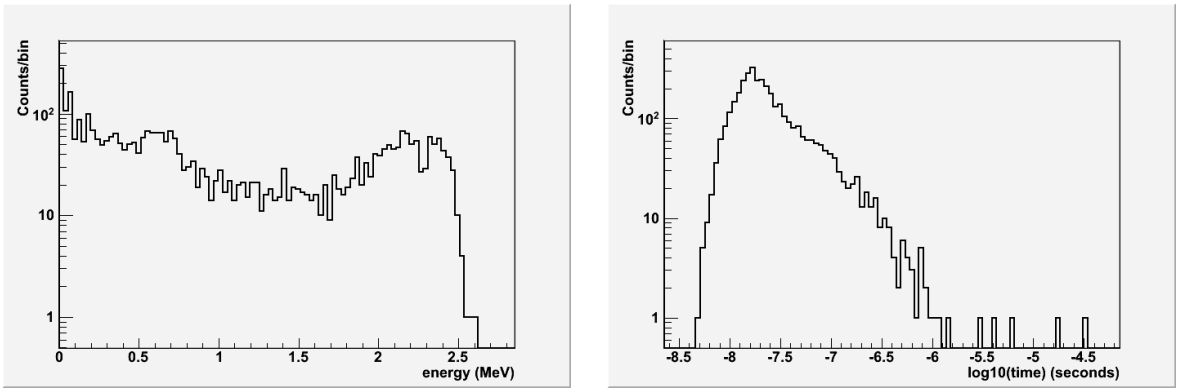

a) b)

Figure 13. Neutron energy spectrum (*a*) and time profile (*b*) obtained by simulating a monochromatic pulse of 10 ns of 2.45-MeV neutrons in the small chamber of the "Bora" device with a 15-cm Fluental TM moderator.

From this picture it is clearly seen that we have fulfilled the above-mentioned conditions. We investigated also some other moderators (e.g. tungsten) and we have also done such works for the 14-MeV neutrons that can be generated in DPF filled with D-T mixture.

2.6. *A single-shot nanosecond neutron pulsed technique for the detection of fissile materials*

In principle there are two methods that can be applied with DPF-generated neutrons due to the fact that spectrum of fission neutrons induced in fissile materials from an external source ("Watt spectrum") covers the range extended from 0.5 till 5.0 MeV with a maximum positioned near 1.5 MeV:

1) To use 2.5-MeV neutrons and look for a component of fission neutrons having energy *higher* than 2.5 MeV

2) To use 14-MeV neutrons and look for a component of fission neutrons having energy *lower* than 14 MeV.

Our MCNP modeling has shown that our neutron yield generated with pure deuterium (10^9 n/shot) is not enough for the first method; so we used 14-MeV neutrons.

Experimental results obtained with the PF-6 device working with D-T mixture on the irradiation of the EK-10 fuel element are shown in Fig. 14 and 15.

From these pictures one may clearly see neutrons elastically and inelastically scattered by elements ingressed into the fuel element. It is essential to note that these oscilloscope traces were obtained just in one shot of our DPF. This single-shot technique of collecting information during about 100 ns is in particular important for application in unveiling of fissile materials hidden in fast-moving objects (cars, trains, ships, etc.).

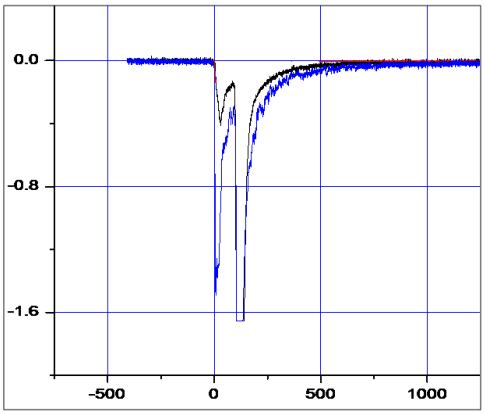

Figure 14. Two oscilloscope traces overlapping one another: one is taken without fuel element (the black one, smooth) and another one is taken with fuel element EK-10 (the blue one with multiple peaks).

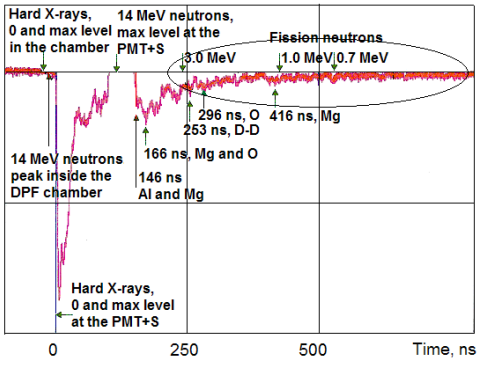

Figure 15. A result of the subtraction of oscilloscope traces with attribution of different peaks and comparison with the results of MCNP modelling calculations.

3. Contemporary scaling laws and drivers for DP foci

Fig. 16 presents a collection of experimental results on neutron and hard X-ray yields obtained to the moment with DPF devices of energy ranged from 1 J till few hundred kJ. We add some possible data using approximations to much higher and much lower currents/energies of the DPF discharge.

As it was found in the end of 80's of the last century for the medium-sized DPF neutron yield scaling may be roughly described by a formula:

$$Y_N \sim n_{pl} N_i (\sigma v) V_{pl} \Delta t \sim I_{pinch}^4 ,$$

where plasma density $n_{pl} = const$, *density of fast ions* $N_i \sim I_{pinch}$, $T_{pl} = const$, Energy Distribution Function of fast ions ~ *const, i.e.* $(\sigma v) \sim const$, $V_{pl} \sim I_{pinch}^2$, $\Delta t \sim I_{pinch}$ – Plasma Confinement Time.

For the hard X-ray yield the situation is a bit more complicated due to the facts that we have in DPF not just an electron beam but relativistic electron plasma ($v/\gamma >> 1$) and the absorption (deceleration) of fast electrons in the anode's material is accompanied by a collective plasma mechanisms and by a so-called "magnetic stopping" within the anode's plasma. But roughly:

$$Y_X \sim I_{pinch} U^2 Z_{anode} \tau_e \sim I_{pinch}^2 ,$$

where $U \sim E_i$ (more precisely speaking the distribution function of fast electrons) ~ *const*, $\tau_e \sim I_{pinch}$.

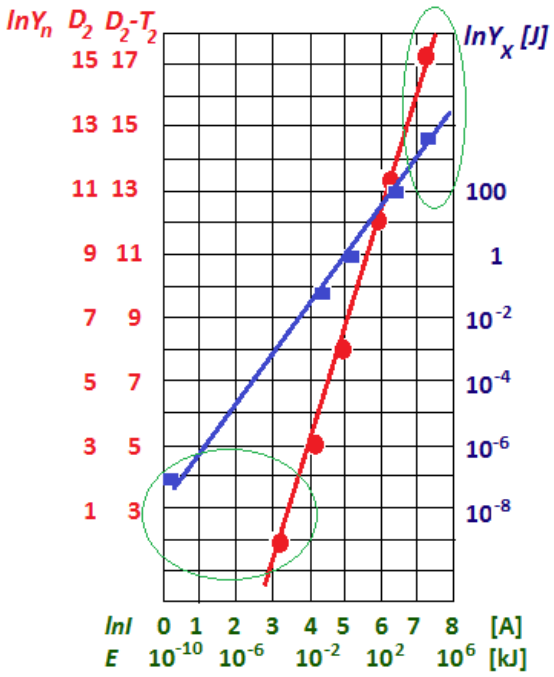

Figure 16. Experimental scaling for neutron and X-ray production in DPF. Regions in a circles has not been reached yet.

DPF is a high-current accelerator producing nanosecond pulses of fast particles without expensive and cumbersome intermediate elements of the type of PULSE FORMING LINES (e.g. the Blumlein line) that are not very reliable in exploitation, very expensive and have problems at their exploitation with a high repetition rate. However in the case of *large DPF devices* the usage of the in-between elements as in a classical scheme of high-current high-voltage generators (see e.g. in Fig. 17 a design map of GAMMA facility) might be productive from the point of view of matching all elements of it.

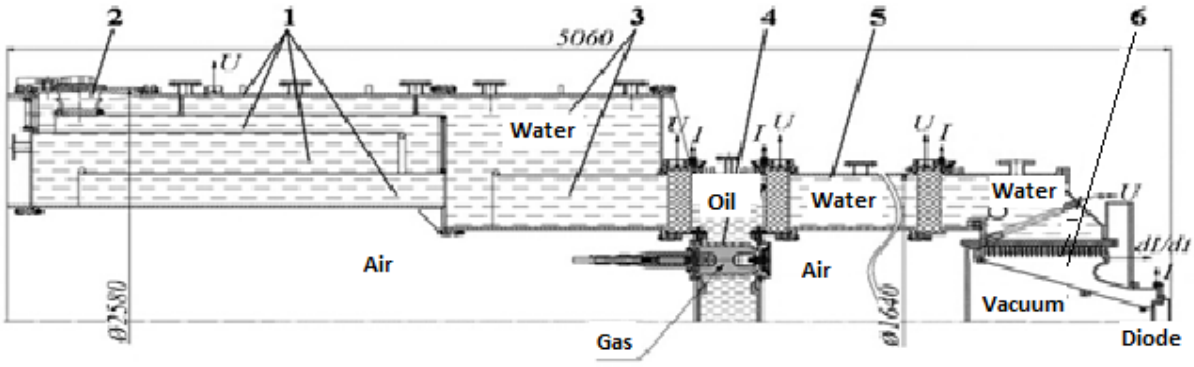

Figure 17. Design map of a high-voltage section of accelerator with a high-current vacuum diode (GAMMA facility, Sarov, R.F.): 1 – the first four double-stepped forming line – DSFL – cascades, 2 – DSFL multichannel switch, 3 – DSFL output cascade with a built-in duration converter, 4 – pre-pulse switch, 5 – WTL, 6 – vacuum insulator with MITL and vacuum diode.

Indeed after current abruption taking time of about an inverse increment of Langmuir plasma instability (in ps range) a DPF chamber of the Mather geometry is nothing more than a Transmission Line with Magnetic Insulation (MITL – see Fig. 18) where the overall e/m energy is transported as a e/m wave to the plasma diode as it is realized in the above Fig. 17. So in the case of a very large DPF it is impossible to expect a fulfillment of a good matching of current generator (primary energy storage) with the plasma diode.

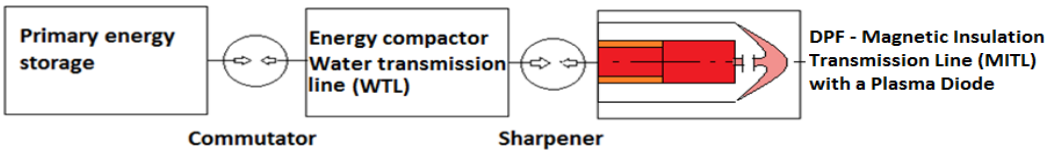

Figure 18. DPF with intermediate matching element.

In this case due to this intermediate element we can match the primary energy source with the load much easier. E.g. at the use of a double forming line (DFL – the so-called Blumlein line) the value of power released at the DPF will be (see e.g. [10]):

$$P_R = \frac{4U^2R}{(R+\rho)^2} = c\sqrt{\frac{\varepsilon}{\mu}}\,\frac{4E_m{}^2R_1^2\ln^2(R_2/R_1)}{2(\ln(R_2/R_1)+\ln(R_3/R_2))}\,\frac{R\rho}{(R+\rho)^2} = c\sqrt{\frac{\varepsilon}{\mu}}\,\frac{2E_m{}^2R_3^2\ln(X)}{X^2+X}\,e^{-\frac{2}{X}\ln X}\,\frac{R\rho}{(R+\rho)^2}$$

where E_m – maximal electric field in the line, R – load resistance (DPF's diode), R_i – radii of coaxial conductors of the line, $\rho = \rho_1 + \rho_2$ – summarized wave impedance of the line, $X = R_2/R_1$. By changing X it is possible to match DFL with DPF. Maximal power will be released in DPF at X = 1.52.

However at the numerical modeling of these schemes the full set of MHD equations must be used together with the *equations of telegraphy* at the final stage instead of simple electrotechnical equations of C-L-R circuitry to describe electro-magnetic wave travelling along the MITL.

Understanding the problems of matching of big devices with a large-scale DPF chamber in general and with its diode in particular as well as the problem of spending too much energy for the rundown phase in big DPF facilities we took out three patents (Fig. 19) in the beginning of 80's [11] with the following ideas:

1) Usual contemporary 1-MW electric power turbine has U = 30 kV and I = 30 kA. We may use transformer to change 30 kV into 10 V. In this case we shall obtain the output current I = 90 MA. We may use here an invertor (or convertor) to fit (match) operation frequency to the travelling time of the current sheath inside the DPF chamber, and/or -
2) To initiate the discharge by means of a laser pulse not to spend too much energy for the rundown phase (or to use one or several small DPF):

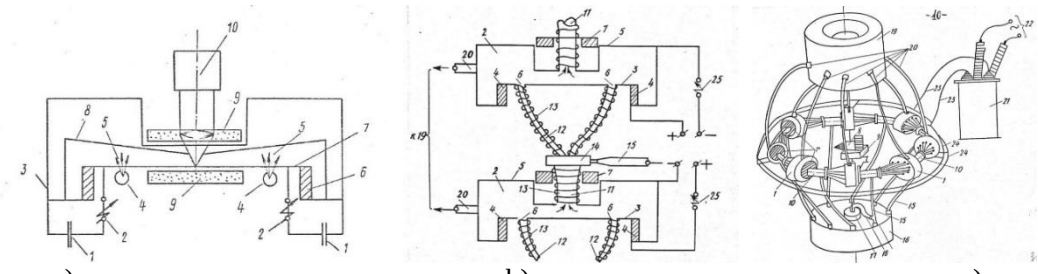

Figure 19. 3 modifications of DPF or their chains to overcome problems with energy loss for a rundown phase.

Two important issues are raised in such schemes:

1) Whether recovering of electric insulation between anode and cathode of a DPF chamber after the discharge (or better to say a disconnection between the DPF chamber and primary source of energy) is possible?
2) How much power may we extract from the mains?

The answer to the first question has been obtained in our experiments. Namely, the interruption of current circulating in a DPF circuit may be ensured either in pseudo-spark switches (PSS) usually used by us [12] (see Fig. 20*a* and *b*) or directly in a gap between the anode and the cathode of the DPF chamber (as it is seen in Fig. 20*c* – during the pinch phase – and 20*d* – 10 μs later the CA phenomenon if the space above the anode is large enough).

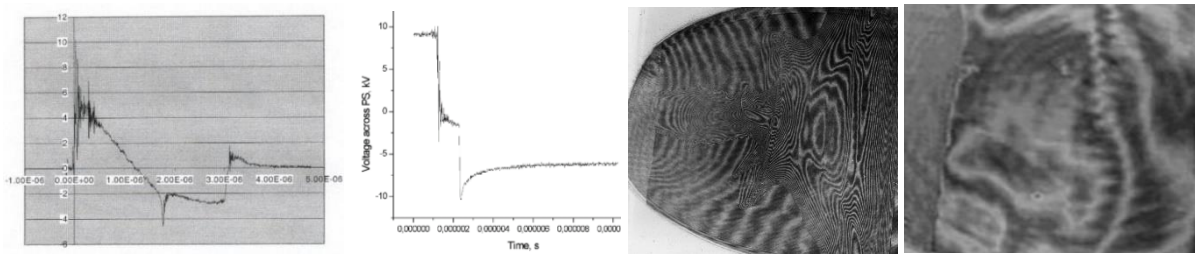

a) b) c) d)

Figure 20. PSS's disconnection: current (*a*) and voltage (*b*); blow-off of plasma in PF-1000: moment of the dip (*c*) and 10 μs later (*d*).

According to electric power generation laws an allowable unsinusoidality of the current generated may be not more than 5%. This demand implies the restriction upon our "dip" and consequently on the extracted power if we want to use the rest power to feed the common mains.

4. Possible applications of a very large DPF

4.1. *Medicine*

In previous paragraphs we have discussed a possibility of application of a DPF for the low-dose high intensity *single shot* neutron therapy of cancer. The characteristics of the radiation fields in this case of 'classical BNCT' by epithermal neutrons are as follows: neutron intensity on the tumor surface is 10^9 n cm^{-2} s^{-1}; time of irradiation – 40…60 min; dose – 60…70 Gy. It means that the overall neutron fluence is on the level of $3…5\times10^{12}$ n cm^{-2} and the dose rate is equal to 1 Gy·min^{-1}.

Unfortunately the present-day boron preparations are capable to increase concentration of boron atoms within the malignant cells by 3-5 times higher compared with normal cells only (instead of demanded figure equal to 20).

Large DPF (a few MJ) can ensure the dose power on the level exceeding 10^9 Gy/min at a neutron pulse of ~ 100-ns duration. For this we need a neutron flux ~ 10^{12} n/cm^2 acting during a time interval << the reaction time with Li, α and free radicals (i.e. < 1 μs). In this case we shall overcome the above-mentioned *threshold* in malignant cells *only*. Because of this we shall increase *selectivity*, and we shall be able to *decrease the overall fluence* by an order of magnitude, thus providing *treatment just in a single pulse*.

4.2. *Radiation material sciences*

One of the possible exploitations of DPF as a powerful source namely of *fusion* neutrons in material sciences is its use as the source for testing of materials perspective for the first wall components and construction elements in the magnetic confinement fusion and in the inertial confinement fusion reactors where the neutron interaction with materials will be of the "explosive-like" type.

The IFMIF (~10^9 US$) as expected will be able to ensure during one year of irradiation *the neutron fluence on the level from 0.01 till 50 displacements per atom* (dpa) in various zones positioned near a target having the area 5×20 cm^2. The value of 1 dpa corresponds to the fluence of 10^{21} n/sm^2 for Be- and C-based materials.

If in the DPF facility the pinch current would be about 20 MA its neutron yield will exceed 10^{17} of the 14-MeV neutrons. Taking into consideration a possible geometry of the near-pinch anode part of the DPF of this energy level it is easy to estimate that 100 dpa can be succeeded during an operational year in a volume of about 1 liter with the irradiation area ~ 0.1 m^2. But for all that a DPF must work with a repetition rate 3-4 cps with the irradiating zone positioned 0.1 m apart from specimens. Such a device would be cost 100 times less compared with IFMIF in spite of the fact that during this experiment we shall have to change elements of the facility 10 time during the year.

4.3. *Energetics*

Let us assume a DPF device with energy consumption during the shot on the level 30 MJ (so the overall amount of energy circulated within the facility is about 100 MJ). Such DPF may produce about 5×10^{17} n/pulse (~ 1 MJ in neutrons). We have made calculations for the hybrid reactor with a fission blanket having 100 time coefficient of gain [13] (see Fig. 21).

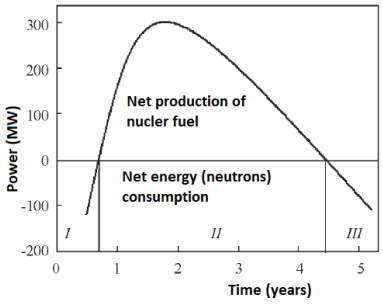

Figure 21. Evolution of energy in a hybrid reactor based on a DPF facility

We obtained the following parameters for the thermal power of the reactor equal to 0.5-1.0 GW and the operation period 2-5 year, efficiency of the fuel cycle 0.4, blanket thickness (for pure U^{238}) 12 cm and thickness of the SS wall 2 cm: uranium mass = 0.8-4 t, mean radius of energy zone is 0.33 m, mean operation rate of the DPF device is 13 cps, mean electric power consumed by the neutron source = 100-300 MW, mean useful electric power at the output = 270 MW. DPF size will be about 2.5 m.

However before reaching by the reactor of the positive value of the energy balance it will consume 6×10^8 kilowatt-hours of electric energy. This is an atonement for the low efficiency of the DPF-based neutron source. But we may use for this purpose the hydro-electric power generated in an estuary of a river in Siberia (see Fig. 22).

a) b) c)

Figure 22. Map of Siberia (*a*), Lena's estuary (60 km) (*b*) and Siberia by night (*c*)

Indeed, in these places because of a very large width of a river (*b*) a power dam may be very low (just 1-3 meters by height). It is good from ecological point of view. But before it was not used as in these regions of Russia are almost uninhabited (*c*). And transportation of electric energy from these territories to industrial regions or delivering of raw materials to these areas are economically ineffective. However with the above-described hybrid nuclear power stations we may interrupt the campaign at its summit and deliver a fission fuel to the industrial territories by a single ship per year.

5. How small a DPF can be?

From the above-presented scaling diagram one may see that at the values of the discharge current of DPF on the level of about 1 A we cannot expect any neutron yield. However the "hard X-ray" yield could be of the order 10^{-8} J that means up to 10^7 hard X-ray photons irradiated in full solid angle!

Pulse duration can be estimated using present day data on this parameter in the range of the bank energy 10^6 down to 1 J. It appears that this duration will be in the range 0.1 – 1 ps. This time is of the order of the increment of Langmuir turbulence presumably responsible for the current abruption phenomenon. So it is feasible.

Size of electrodes of such a device can be calculated using the Lee parameter. It appears that this "facility" will be in a sub-micrometer range of dimensions. With these dimensions the problem of ion saturation current becomes profound: in each successive shot we shall have or have not ion component. To support it we must change polarity and sputter a layer saturated with working gas. It means that such a source of the type of "current breaker" can be inserted in modern microchip structures. Manufacturing of these elements should be provided using micro-mechanics technology, e.g. with the help of medium-sized DPF working with Ar as a working gas.

6. Opportunities for a miniature DPF

In his 1971 paper, Chua extrapolated the conceptual symmetry between the resistor (voltage vs. current), capacitor (voltage vs. charge), and inductor (magnetic flux vs. current), and inferred the *memristor* [14] (see Fig. 23) as a similarly fundamental circuit element *linking magnetic flux and charge.* In contrast to a linear (or nonlinear) resistor the memristor has a dynamic relationship between current and voltage including a memory of past voltages or currents.

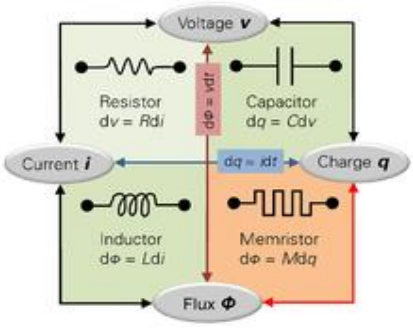

Figure 23. Zone occupied by a memristor in the symmetrical scheme of passive electrical elements.

Device	Characteristic property (units)	Differential equation
Resistor	Resistance (V per A, or Ohm, Ω)	$R = dV / dI$
Capacitor	Capacitance (C per V, or Farads)	$C = dq / dV$
Inductor	Inductance (Wb per A, or Henrys)	$L = d\Phi_m / dI$
Memristor	Memristance (Wb per C, or Ohm)	$M = d\Phi_m / dq$

The resistance of a memristor depends on the *integral* of the input applied to the terminals, i.e. on the charge coming through it (rather than on the *instantaneous value of the input* as in a varistor). For some memristors, applied current or voltage will cause a *great change in resistance*. Such devices may be characterized as switches by investigating the time and energy that must be spent in order to achieve a desired change in resistance.

E.g. the HP memristor device is composed of a thin (50 nm) titanium dioxide film between two 5 nm thick electrodes, one Ti, the other Pt. Initially, there are two layers to the titanium dioxide film, one of which has a slight depletion of oxygen atoms. The oxygen vacancies act as charge carriers, meaning that the depleted layer has a much lower resistance than the non-depleted layer.

When an electric field is applied, the oxygen vacancies drift, changing the boundary between the high-resistance and low-resistance layers. Thus the resistance of the film as a whole is dependent on *how much charge* has been passed through it in a particular direction, *which is reversible* by changing the direction of current.

One of the resulting properties of memristors is the existence of a pinched hysteresis effect (see Fig. 24).

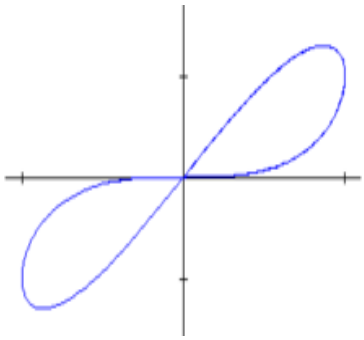

Figure 24. For a current-controlled memristive system, the input *x(t)* is the current *i(t)*, the output *y(t)* is the voltage *v(t)*, and the slope of the curve represents the electrical resistance.

The change in slope of the pinched hysteresis curves demonstrates a switching between different states of resistance, which is a phenomenon central to ReRAM and other forms of two-terminal resistance memory.

Following to these descriptions we may suppose that nano-sized foci may use the following opportunities to be counted (or hereafter used) as memristors:

1) DPF really is a circuit element *linking magnetic flux and charge:* $M = d\Phi_m / dq$ (the higher charge in a capacitor – the bigger values of current and reciprocal magnetic field)
2) Because of a very small size of the chamber we can control a discharge in time at any stage thus making *linkage between charge flowing through and magnetic flux*
3) We may use *ion saturation current effect* (in an analogy to the depletion of oxygen atoms in the titanium dioxide film of a HP© memristor that is under construction)
4) We may exploit a *great change in resistance* taking place twice in the DPF dynamics – in the breakdown phase and during CA phenomenon.

However additionally we may take *advantage from radiation properties* of this miniature DPF device. Indeed, because the overall number of hard X-ray photons is not small we can organize an electrical circuit in such a manner that this X-ray photon flux from DPF will open (or close) locally semiconductor elements (e.g. diodes or transistors) just through the space, i.e. without electrical connections. It can be done by interaction of X-rays with a semiconductor material and creation of uncombined carriers in the surrounding elements of a microchip.

In some cases it will be very important thus making such a memristor not simply a *passive element* of the circuitry but the *active one*.

7. Conclusions

With the above speculations we can see that in future there is a quite imaginable probability to gain prospects for:

1) Production of energy with *huge DPF facilities*

2) Implementation of these *large DPF facilities* in medicine for a *single-shot low-dose cancer therapy*

3) Use *this energy for feeding medium-sized DPF devices* that could be applied in different applications – radiation material sciences, biology, medicine, dynamic quality control, *single-shot* interrogation of illegal objects, but in particular for manufacturing of *very tiny elements of sophisticated computers* including super-miniature DPF as the parts of them

4) In the last case we may obtain IT technique not only with the super-miniature *passive* elements in its content but with the *active* ones.

8. Acknowledgments

This work was partially supported by the International Atomic Energy Agency CRP grants numbers RC-16932, RC-16954, RC-16955, RC-16956, RC-16960, RC-17167.

9. References

[1] Bernard A., H. Bruzzone *et al* 1998 *J. Moscow Phys. Soc.* **8** 1–93
[2] Gribkov V.A., Bienkowska B., Borowiecki M. *et al* 2007 *J. Phys. D: Appl. Phys.* **40** 1977–89
[3] Gribkov V.A., A. Banaszak, B. Bienkowska *et al* 2007 *J. Phys. D: Appl. Phys.* **40** 3592–607
[4] Kingsep A.S., Chukbar K.V. and Yan'kov V.V. 1987 Electron magnetic hydrodynamics *Voprosy Teorii Plazmy (Problems of Plasma Theory)* ed. by B.B. Kadomtsev **16** (Moscow: Energoatomizdat) 209 (in Russian)
[5] Gribkov V.A., Orlova M.A. 2004 *Radiat. Environ. Biophys.* **43** 303–309, DOI 10.1007/s00411-004-0259-2
[6] Gribkov, Lee S., Lee P. *et al* 2000 ISMA-2000: International Symposium on Microelectronics and Assembly, 27 November - 2 December 2000, Singapore
[7] Gribkov V.A., Lee S. *et al* 2000 Proc. of the ICPP-2000: International Congress on Plasma Physics, 42nd Annual Meeting of the Division of Plasma Physics of the American Physical Society, October 23 - 27, 2000, Quebec City, Canada
[8] Orlova M.A., Kost O.A., Gribkov V.A. *et al* 2000 *Applied Biochemistry and Biotechnology* **88** 243-55
[9] Giannini G., Gribkov V., Longo F., Ramos Aruca M. and Tuniz C. 2012 *Phys. Scr.* **86** 055801 (9pp) doi:10.1088/0031-8949/86/05/055801
[10] Arzhannikov A.V., Sinitskij S.L., Powerful pulsed beams, Teaching aid, Novosibirsk State University, 2007, 74 pp. (in Russian)
[11] Gribkov V.A., Tyagunov M.G., USSR patents Nos. 1012707 (26.01.1981), 1026439 (01.03.1981) and 1101838 (20.12.1982) (in Russian)
[12] V.A. Gribkov, M. Scholz, V.D. Bochkov *et al* 2004 *J. Phys. D: Appl. Phys.* **37** 2107-2111
[13] Gribkov V.A., Tyaganov M.C., Possible applications of a hybrid thermonuclear source based on the DPF device in modern energy complexes. – Nuclear Technologies in a Sustainable energy System, ed. by G.S. Bauer and A. McDonald, 1983, Springer-Verlag; B.,H., N.-Y.; 187-202
[14] http://en.wikipedia.org/wiki/memristor